Dielectric Rod Antenna With Third-Harmonic Suppression via Photonic Crystal Bandgap Material

Simon P. Hehenberger, *Graduate Student Member, IEEE*, Stefano Caizzone, *Member, IEEE*, and Alexander Yarovoy, *Fellow, IEEE*

***Abstract*—A novel concept to mitigate the unintended transmission and reception of signals at the third harmonic of dielectric rod antennas is proposed. To suppress the third-harmonic radiation, an additive-manufactured photonic bandgap material is used in the dielectric rod antenna. The antenna has been designed to operate at the frequency of 5 GHz and exhibit a bandgap at the third-harmonic frequency of 15 GHz. The design of the material is explained via the band diagram of the bandgap material and imperfections introduced due to the additive manufacturing (AM) process considered. Numerical simulations of dielectric rod antenna prototypes fed via a rectangular waveguide (RWG) with and without harmonic suppression are carried out to confirm the operational principle. The design proposed is verified experimentally. The manufactured antenna is characterized in terms of its input reflection coefficient and far-field radiation properties. The obtained experimental results agree well with predictions obtained through simulations and confirm the third-harmonic suppression capability of the antenna.**

***Index Terms*—Additive manufacturing (AM), antenna, bandgap, dielectric crystal, dielectric rod, harmonic suppression.**

I. Introduction

MODERN communication and sensing systems are currently targeting higher and higher frequencies in order to satisfy the increasing bandwidth requirements. This trend to higher frequencies does come with unique challenges. For one, equipment operating at millimeter wave (mmWave) frequency bands suffers from higher conductive losses than their low-frequency counterparts. Therefore, the application of current state-of-the-art printed circuit board (PCB) technology severely hinders the complexity of high-frequency equipment and, most importantly, the obtainable efficiency. Another challenge with the push of applications into the mmWave regime is the spectrum crowding and signal integrity issues arising from the increased utilization of high-frequency bands. In recent years, low-cost additive manufacturing (AM) of dielectric antennas has received increased attention due to its potential to address the limitations posed by planar antennas based on subtractive PCB manufacturing technologies. Although it does not provide the best accuracy, the fused filament fabrication (FFF) approach is desirable due to the low cost of the process and the potential for multimaterial dielectric manufacturing. For example, dielectric resonator antennas have been proposed as a viable alternative to microstrip patch antennas due to their flexibility in design, the capability of miniaturization, and high radiation efficiency [1], [2]. Another type of dielectric antenna, the dielectric rod antenna, is a suitable candidate to achieve high gain and efficiency while also providing a smaller footprint and increased flexibility in manufacturing when compared to microstrip-based antenna systems with similar gain. The dielectric rod is usually a solid dielectric structure integrated with waveguide or planar feeds to increase the directivity of the feed structure and has been thoroughly investigated [3]. However, dielectric rod antennas are wideband and radiate independent of the excitation mode and are therefore susceptible to unintended radiation or reception of signals at the third harmonic of the system, which might cause issues with signal integrity or out-of-band radiation. In a wireless communication system, a harmonic suppression filter between an antenna and a power amplifier is a convenient way to suppress electromagnetic interference [4]. However, such filters are usually bulky, expensive, and challenging to integrate, which leads to approaches integrating harmonic control via microstrip shorts and pins [5] and photonic bandgap materials [6]. In this work, a novel approach is utilized to effectively suppress the radiation and reception of signals at the third harmonic in dielectric rod antennas without additional components. This is achieved by additively manufacturing the dielectric rod as a photonic crystal that behaves like an effective medium at the design (fundamental) frequency but exhibits a complete 3-D bandgap at the third harmonic. Photonic crystals exhibiting complete 3-D bandgaps have first been introduced by Yablonovitch [7]. However, they are difficult to manufacture with traditional subtractive methods and thus have not received much attention for actual applications. Furthermore, their size with respect to the wavelength has been unattractive for antenna applications so far. However, the move to mmWave frequencies and AM being ideally suited to create complex 3-D dielectric structures makes the utilization of photonic bandgap materials viable for

Received 30 July 2024; revised 22 February 2025; accepted 7 April 2025. Date of publication 2 June 2025; date of current version 6 August 2025. *(Corresponding author: Simon P. Hehenberger.)*

Simon P. Hehenberger is with the German Aerospace Center Institute of Communication and Navigation, 82234 Weßling, Germany, and also with the Microwave Sensing, Signals and Systems Department,Delft University of Technology, 2628 CD Delft, The Netherlands (e-mail: simon.hehenberger@dlr.de).

Stefano Caizzone is with the German Aerospace Center Institute of Communication and Navigation, 82234 Weßling, Germany (e-mail: stefano.caizzone@dlr.de).

Alexander Yarovoy is with the Microwave Sensing, Signals and Systems Department, Delft University of Technology, 2628 CD Delft, The Netherlands (e-mail: a.yarovoy@tudelft.nl).

Digital Object Identifier 10.1109/TAP.2025.3573601

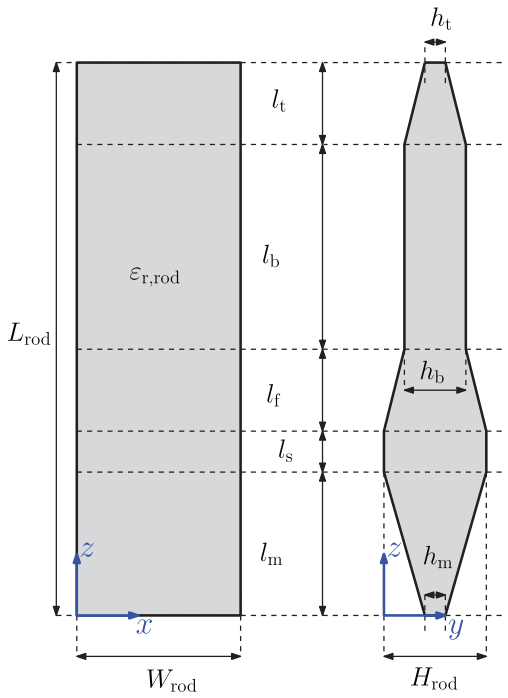

Fig. 1. Geometry of the proposed dielectric rod.

TABLE I
GEOMETRIC PARAMETERS OF THE PROPOSED DIELECTRIC ROD ANTENNA

L_{rod}	191,84 mm	l_s	10mm	h_m	2,54 mm
$a_{RWG} = W_{rod}$	47,55 mm	l_f	36,54 mm	h_b	10,53 mm
$b_{RWG} = H_{rod}$	22,15 mm	l_b	55,30mm	h_t	5 mm
l_m	60 mm	l_t	30mm	$\varepsilon_{r,rod}$	2.7

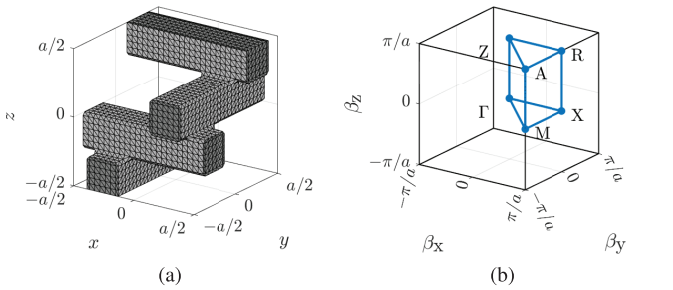

Fig. 2. (a) Woodpile unit cell geometry and its corresponding. (b) Brillouin zone with key points of symmetry.

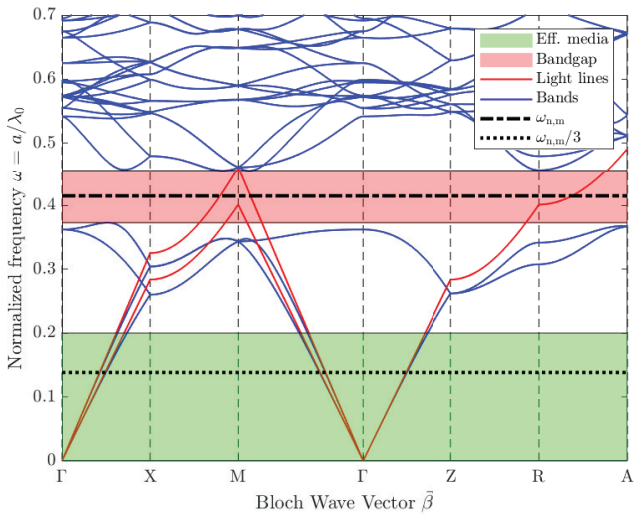

Fig. 3. Band diagram of the woodpile unit cell with visualization of the effective media region (green) and the bandgap (red).

applications in antenna engineering as has been demonstrated in [8].

The rest of the article is structured as follows. Section II introduces the concept and explains a design of a rectangular waveguide (RWG)-fed dielectric rod antenna at 5 GHz. Section III introduces the concept and design of a dielectric crystal based on the woodpile geometry that acts as an effective media at the fundamental and exhibits a bandgap at the third harmonic. Section IV addresses the manufacturing via FFF AM. Section V presents the numerical simulations of the input reflection coefficient and far-field patterns performed with CST Microwave Studio and compares them to experimental results obtained in an anechoic chamber. Section VI provides a conclusion to the presented work.

II. DIELECTRIC ROD ANTENNA

Dielectric-rod antennas, also known as polyrod antennas, are regarded as a type of surface-wave antenna. Their size and weight are very suitable for the millimeter-wave range, and their compatibility with dielectric waveguides opens a wide range of applications [10]. While a wide range of configurations of feeds and rod geometries are possible for the dielectric rod antenna, this work utilizes a simple rectangular-shaped rod with relative permittivity $\varepsilon_{r,rod}$ and linear tapered sections, as shown in Fig. 1. Impedance matching to the feed waveguide is improved via a tapered matching section leading up to the aperture of the feed waveguide. The taper gradually transforms the propagating mode in the waveguide to a surface wave in the dielectric. The feed taper increases the excitation efficiency and influences the feed pattern, while the termination taper reduces the reflected surface wave to negligible values. The efficiency of surface wave excitation is usually between 65 and 75 percent [11], and the feed aperture radiates power not coupled into the surface wave. The rod is designed with a relative permittivity of $\varepsilon_{r,rod} = 2.7$ to exhibit a gain of about 12 dBi at the design frequency $f_d = 5$ GHz while minimizing the rod length and being fed via a standard WR187 RWG with lateral dimensions $a_{RWG} = W_{rod} = 47.55$ mm and $b_{RWG} = W_{rod} = 22.15$ mm. Justification for the design permittivity is provided in Section III. Details about the design of the rod are not repeated here as they are not the focus of this work, and interested readers are referred to [10] and [11]. The geometric parameters of the rod antenna, referenced in Fig. 1 are given in Table I.

III. BANDGAP DIELECTRIC CRYSTAL

Three-dimensional periodic dielectric crystals with a spatially dependent permittivity $\varepsilon(\mathbf{r})$[1] with $\mathbf{r} = [x, y, z]^T$, have

[1]Bold letters symbolizing vectors.

received increasing interest over the last couple of years due to the ability to spatially modulate the permittivity of materials, which has been successfully employed to engineer heterogeneous substrates, dielectric resonator antenna, and graded index lenses. However, all of these devices utilize the dielectric crystal as an effective medium, meaning the wavelength of the applied wave is much larger than the size of the crystal unit cell. This effectively means the wave does not experience the material as structured but rather "sees" an averaged medium with no scattering due to internal features of the medium and linear dispersion. However, as soon as the wavelength of the applied wave approaches the size of the unit cell, this averaging effect breaks down, and nonlinear dispersion effects start to play a significant role in the propagation mechanism of the electromagnetic wave. For specific geometries, this can even result in a band of "forbidden" frequencies in which the propagation constant of the wave is purely imaginary, resulting in an evanescent wave. In this work, we employ this effect to create a bandgap at the third harmonic of the design frequency, resulting in effective attenuation of waves at said frequencies. To this end, we utilize one of the most commonly employed photonic bandgap geometries, the woodpile structure as depicted with its Brillouin zone in Fig. 2. The woodpile geometry has primitive tetragonal lattice symmetry and consists of stacked dielectric bars with relative permittivity $\varepsilon_{r,w}$ against free space. Frequencies of propagating modes in the crystal can be found by solving the eigenvalue problem [9]

$$\nabla \times \left(\frac{1}{\varepsilon(\mathbf{r})} \nabla \times \mathbf{H}(\mathbf{r}) \right) = \left(\frac{\omega}{c_0} \right)^2 \mathbf{H}(\mathbf{r}) \tag{1}$$

as obtained from Maxwell's equation, where $\mathbf{H}(\mathbf{r})$ is the magnetic field (eigenvector) of the propagating mode, c_0 is the speed of light, and ω is the mode frequency (eigenvalue). Here, we utilize the plane wave expansion method (PWEM) to solve (1) for the mode frequencies of a given Bloch-wave vector $\boldsymbol{\beta}$. Iterating this method over a set of wave vectors along the boundary of the irreducible Brillouin zone and plotting the resulting eigenfrequencies against the wave vector gives the band diagram of the geometry. The band diagram corresponding to a woodpile lattice with $\varepsilon_{r,w} = 13.7$ is depicted in Fig. 3, and the justification for the choice of relative permittivity is further explained in Section IV. It is worth highlighting several key aspects of the band diagram. First, for low frequencies $\omega_n < 0.2$, the fundamental mode closely follows the light line. This allows to approximate the behavior of the woodpile lattice as an effective medium with linear dispersion. Additionally, in this effective region, the propagating modes in the directions $\Gamma - X$ (propagation along $\hat{\mathbf{x}}$ or $\hat{\mathbf{y}}$[2]) and $\Gamma - M$ (propagation along $(\hat{\mathbf{x}} + \hat{\mathbf{y}})/\sqrt{2}$) two distinct bands are visible, which implies an effective anisotropy of the woodpile lattice and thus a dependency on the polarization of the wave propagating along these general directions. Second, although propagating modes are present at frequencies in the range of $0.2 < \omega_n < 0.373$, these modes experience significant nonlinear dispersion. And third, one is able to observe an absence of propagating modes between the normalized frequencies $\omega_{n,L} = 0.373$ and $\omega_{n,U} = 0.457$, indicating a full 3-D bandgap with a center frequency $\omega_{n,m}$.

[2]Bold letters with $\hat{}$ symbolizing unit-vectors.

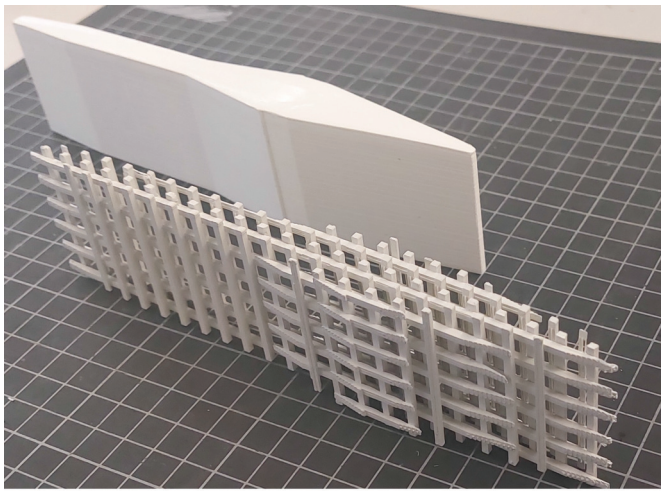

Fig. 4. Manufactured dielectric rod antenna prototypes (back) solid rod made from Ultimaker white PLA and (front) woodpile rod manufactured from Avient ABS1500 material.

The unit cell size of the woodpile lattice a can be designed such that the bandgap center frequency $\omega_{n,m}$, occurs at the third harmonic of the design frequency

$$a = \omega_{n,m}\lambda = \frac{\omega_{n,L} + \omega_{n,U}}{2} \frac{c_0}{3f_d} = 8.3 \text{ mm} \tag{2}$$

where λ denotes the free space wavelength. A woodpile lattice with a lattice constant according to (2) exhibits a bandgap at 15 GHz. The lattice simultaneously behaves as an effective material at the design frequency of 5 GHz, the effective refractive index n_{eff} of the woodpile can be extracted from the band diagram via the technique discussed in [13]

$$n_{eff} = \frac{|\beta|}{k_0} = \sqrt{\varepsilon_{r,eff}\mu_r} \tag{3}$$

with n_{eff} denoting the effective refractive index of the material which for the assumption that no magnetic material is present $\mu_r = 1$ is equal to the square root of the relative permittivity of the material. Applying (3) gives a relative permittivity of $\varepsilon_{r,eff} = 2.7$, which has been used as dielectric rod design permittivity in the previous section. To summarize, the dielectric rod antenna with geometry indicated in Fig. 1 with dimensions given in Table I, comprised of a woodpile lattice made from material with relative permittivity $\varepsilon_{r,w} = 13.7$ and lattice constant $a = 8.3$ mm, should exhibit the same characteristics as one comprised of solid material with relative permittivity $\varepsilon_{r,rod} = \varepsilon_{r,eff} = 2.7$ at the fundamental design frequency $f_d = 5$ GHz. However, the dielectric rod comprised of the woodpile lattice should prohibit any radiation at the third harmonic $3f_d = 15$ GHz due to the full 3-D stopband exhibited by the woodpile lattice at these frequencies.

IV. Manufacturing

Manufacturing 3-D lattices such as the woodpile lattice with traditional manufacturing methods is challenging. However, due to advances in AM over the past decade, manufacturing

such intricate lattices can now be achieved at a comparable low cost and low effort. Besides AM's capabilities, there is a rapidly increasing number of materials compatible with these processes, some of which exhibit high permittivity and low to moderate losses that are well-suited for engineering dielectric bandgap structures. In this work, we utilize extrusion-based AM, where a desired geometry is built layer-by-layer by extruding molten thermoplastic material. One challenging aspect of this technology is that the printing process reduces the relative permittivity of any filament due to unavoidable air gaps between individual lines and layers of the print [12]. Therefore, the dielectric material properties of printed parts need to be experimentally characterized to model the materials accurately. Two materials are employed in this work to manufacture two dielectric rod antennas, one solid and one comprised of a woodpile lattice. The solid dielectric rod is manufactured with polylactic acid filament (PLA) from Ultimaker, exhibiting a measured[3] relative permittivity of $\varepsilon_{\mathrm{r,PLA}} = 2.66$ and a loss tangent of $\tan\delta_{\mathrm{ABS1500}} = 0.062$ [13], which we consider close enough to the design permittivity of $\varepsilon_{\mathrm{r,rod}} = 2.7$ for the purposes of this work. The dielectric rod comprised of a woodpile lattice is manufactured via the ABS1500 material from Avient (former PREPERM), which exhibits a nominal relative permittivity of $\varepsilon_{\mathrm{r,ABS1500,n}} = 15$ and a loss tangent of $\tan\delta_{\mathrm{ABS1500,n}} = 0.018$.[4] In order to estimate the effect of the print process on the dielectric properties of the ABS1500 material, a printed bulk sample was characterized via the Nicholson-Ross–Weir method based on measured scattering parameters within a WR187 RWG. The measured relative permittivity is $\varepsilon_{\mathrm{ABS1500,r}} = 13.7$ with a loss tangent $\tan\delta_{\mathrm{ABS1500}} = 0.02$, which is the effective permittivity utilized in the design of the woodpile lattice $\varepsilon_{\mathrm{r,w}}$ in the previous section. The manufactured prototypes of the solid and woodpile dielectric rod are depicted in Fig. 4.

V. Simulation

To confirm the operational principle of the proposed antenna, numerical analysis of the RWG -fed dielectric rod antenna is carried out with CST Microwave Studio for three individual cases. One for the standalone RWG, one for the waveguide-fed dielectric rod antenna with dimensions given in Fig. 1 and Table I, and one for the waveguide fed dielectric rod antenna where the dielectric rod body is intersected with the woodpile lattice. The 3-D models for the latter two cases are depicted in Fig. 5.

The intended working principle of the woodpile dielectric rod can be well observed in the comparison of the electric fields inside the solid and woodpile dielectric rod antennas at 5 and 15 GHz in Fig. 5(c)–(f). The electric field distribution in the solid and woodpile rod are similar at the design frequency at 5 GHz, but the woodpile strongly attenuates the field at 15 GHz due to the presence of a stopband. The radiated power and reflection coefficient as a function of frequency, as well as the realized gain patterns at the fundamental and third harmonic, are compared for the three individual cases for the excitation of the fundamental mode in the waveguide in Fig. 6. From the reflection coefficient and the radiated power in Fig. 6(a) and (b), it can be well observed that the woodpile dielectric rod is effective in suppressing radiation between 10 and 16 GHz, compared to the solid rod and standalone waveguide. Furthermore, as intended, the woodpile rod mimics the

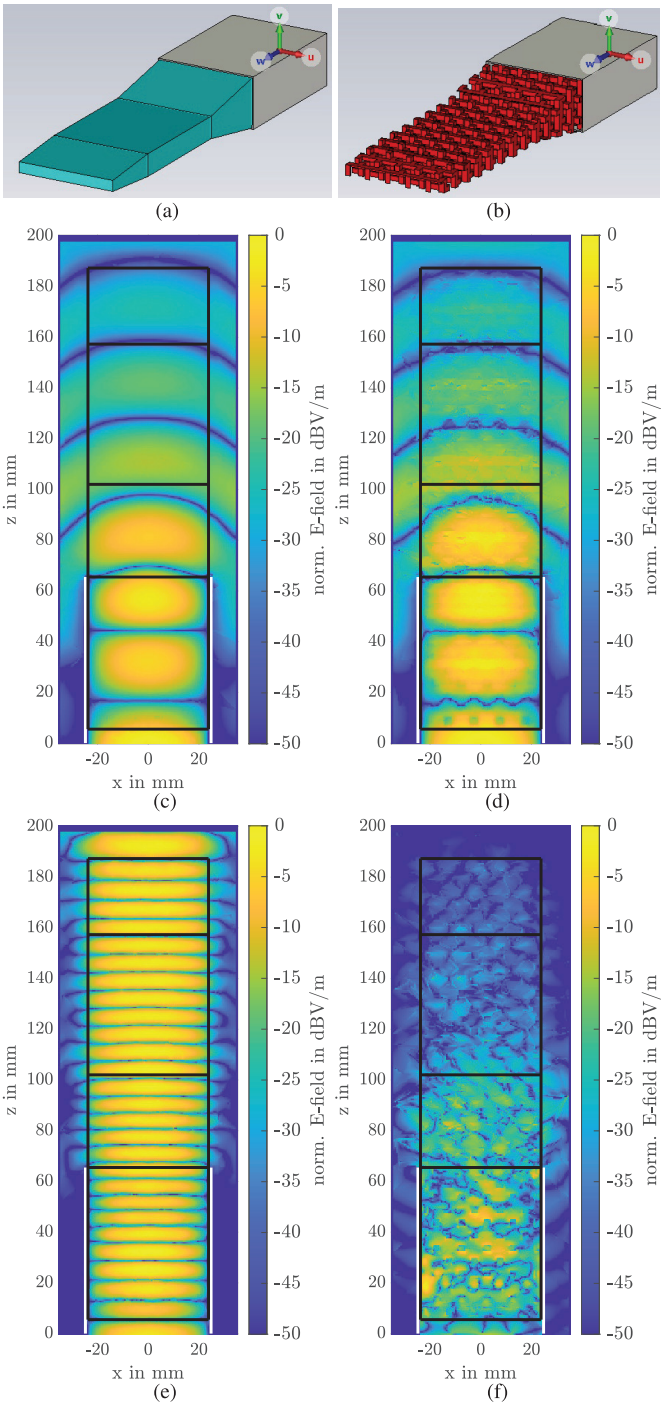

Fig. 5. CST Microwave Studio models for the dielectric rod antenna with RWG feed in (a) solid-material permittivity $\varepsilon_{\mathrm{r,rod}} = 2.7$, (b) woodpile-material permittivity $\varepsilon_{\mathrm{r,w}} = 13.7$ configurations and normalized simulated electric field values in the solid (c) and (e) and woodpile (d) and (f) rod antennas at (c) and (e) 5 GHz and (d) and (f) 15 GHz in the xz-plane where the waveguide dimensions and rod dimensions are indicated as white and black lines, respectively.

[3]No nominal permittivity is mentioned in the datasheet of this material.
[4]Datasheet available from the manufacturer upon request.

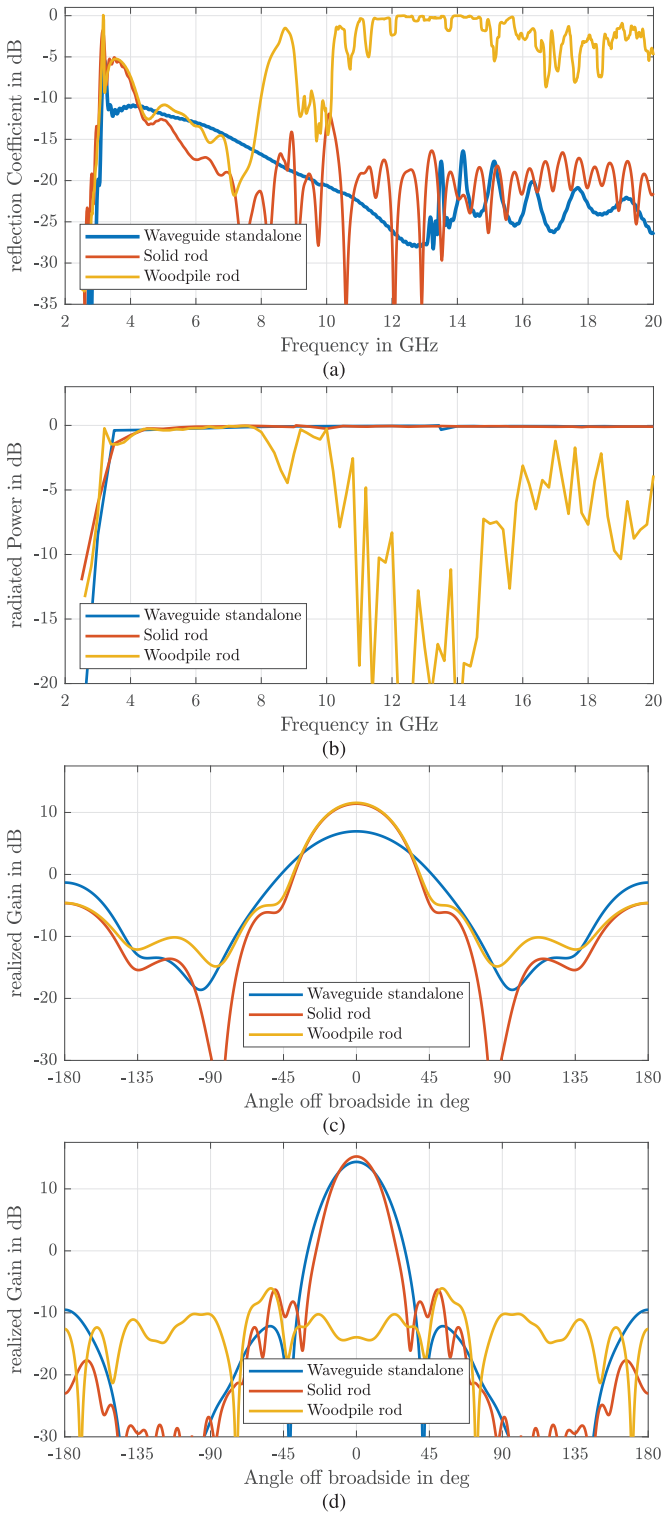

Fig. 6. Simulation results of the different antenna configurations. Standalone waveguide (blue), the solid dielectric rod (red), and the woodpile dielectric rod(yellow) configurations. (a) Reflection coefficient of the rectangular waveguide waveport. (b) Radiated power and co-polarized realized gain radiation patterns at (c) design frequency (5 GHz) and (d) its third harmonic (15 GHz).

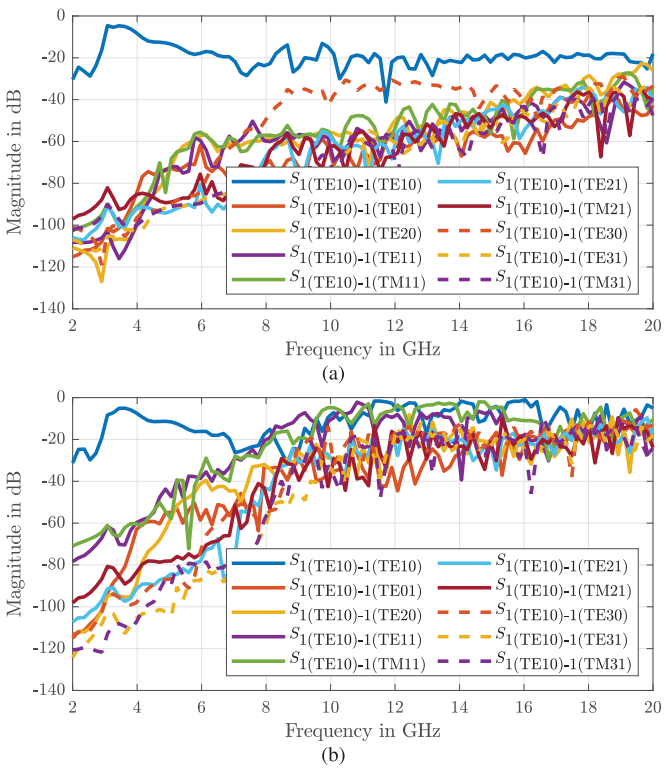

Fig. 7. Multimode scattering parameters of the waveguide-fed dielectric rod antenna with respect to the fundamental mode in the waveguide (TE10) for (a) solid and (b) woodpile rod, as a function of frequency.

characteristics of the solid rod at lower frequencies between 4 and 7 GHz. This is also well observed with respect to the realized gain in Fig. 6(c) and (d), respectively. At 5 GHz, both the solid and woodpile rod exhibit the desired increase in gain of about 5 dB compared to the standalone waveguide and have almost identical radiation patterns. However, at 15 GHz, the realized gain of the woodpile rod is ≈30 dB lower at broadside compared to the solid rod and the standalone waveguide. Nevertheless, there is also a noticeable increase in realized gain for angles between 60 and 140 degrees off the broadside. While no difference in the front-to-back ratio between the solid and woodpile rod is observed at the design frequency, there is a degradation of ≈9 dB of it at the third harmonic. Generally, it appears the bandgap does not center at the desired frequency of 15 GHz but around 13 GHz. The difference might be caused by an insufficient converged band diagram of the PWEM, resulting in small errors in the estimated bandgap frequencies and corresponding unit cell size in (2). Furthermore, some unexpected behavior is worth highlighting. There is an increase in the reflection coefficient and corresponding drop in radiated power between 8 and 9 GHz for the woodpile rod compared to the solid rod, which does not seem to correspond to the stopband of the woodpile structure. Consulting the band diagram in Fig. 3, one can observe that this frequency range falls between the bandgap and effective media frequency regimes, where the fundamental mode in the woodpile lattice experiences nonlinear dispersion and interaction with higher order modes in the woodpile lattice. To further study this behavior, a multimode simulation for the first ten propagating waveguide modes has been carried out, and the corresponding scattering parameters with respect to the fundamental mode are depicted in Fig. 7 for the solid and woodpile dielectric rod, respectively. One is able to observe an increased coupling into the higher order modes in

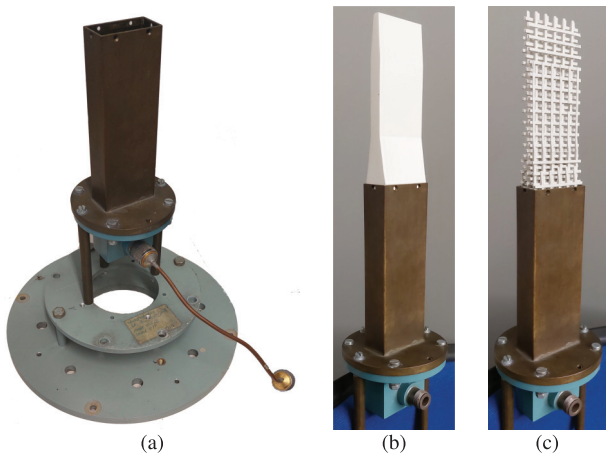

Fig. 8. Measured antenna configurations. (a) Standalone RWG with mounting plate. (b) Solid dielectric rod inserted into the waveguide aperture. (c) Woodpile dielectric rod inserted into the waveguide aperture.

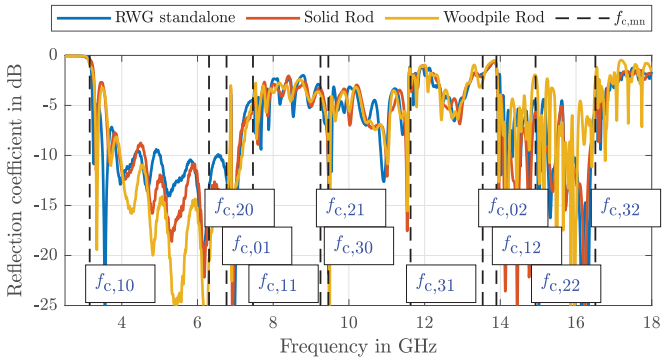

Fig. 9. Measured input reflection coefficient of the RWG standalone (blue), with the solid dielectric rod antenna (red) and with the woodpile dielectric rod antenna inserted into the waveguides aperture and cut-off frequencies f_{mn} of individual TE_{mn} modes in plotted in black dashed lines and labeled in blue.

the simulated scattering parameters of the woodpile dielectric rod compared to the solid rod. Already at the design frequency, an increased scattering to the TE11 and TM11 is noticeable. Furthermore, a significantly increased coupling to higher order modes is found at frequencies where the woodpile cannot be approximated as an effective medium with linear dispersion anymore. This phenomenon could explain well the unexpected rise in the reflection coefficient and corresponding drop in radiated power observed between 8 and 9 GHz in the single-mode simulations in Fig. 6(a) and (b) respectively.

VI. Measurement

The three antenna configurations discussed in the numerical simulations are now also considered in an experimental setup and characterized in terms of their input reflection coefficient and their far-field radiation patterns. The RWG utilized for the measurement is a standard WR187 with a length of 150 mm and fed via a coaxial transition with an N-type connector. The individual rod antenna prototypes are inserted into the waveguide aperture as depicted in Fig. 8. Antenna measurements are carried out with the individual antennas in receiving configuration and under far-field conditions in the Delft University Chamber for Antenna Tests (DUCAT) for a frequency range of 2.5–20 GHz. The measured input

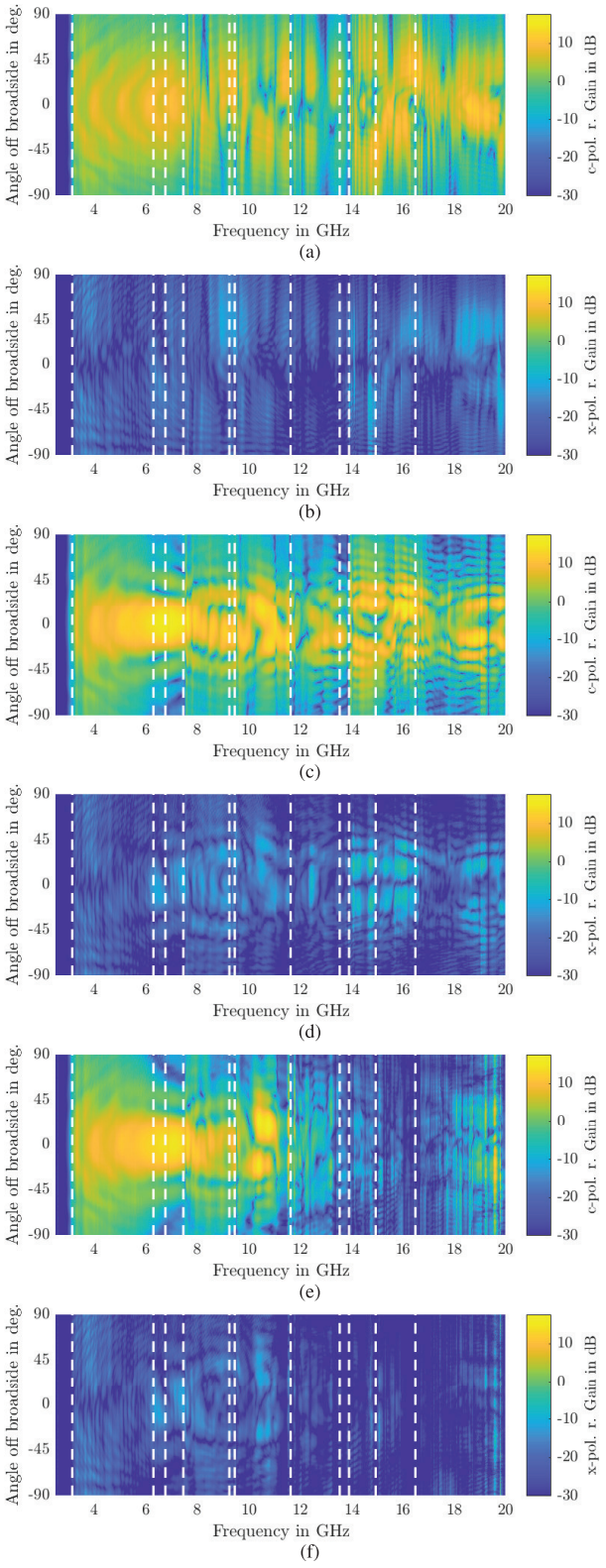

Fig. 10. E-plane co- (a), (c), and (e), and cross-polarized (b), (d), and (f) realized gain measurements as a function of frequency and angle of broadside for (a) and (b) standalone RWG, (c) and (d) solid dielectric rod and (e) and (f) woodpile dielectric rod antenna with the cut-off frequencies of individual higher order modes in the waveguide plotted in dashed white lines.

reflection coefficients, as depicted in Fig. 9, are dominated by the reflection of the coaxial to waveguide transition employed

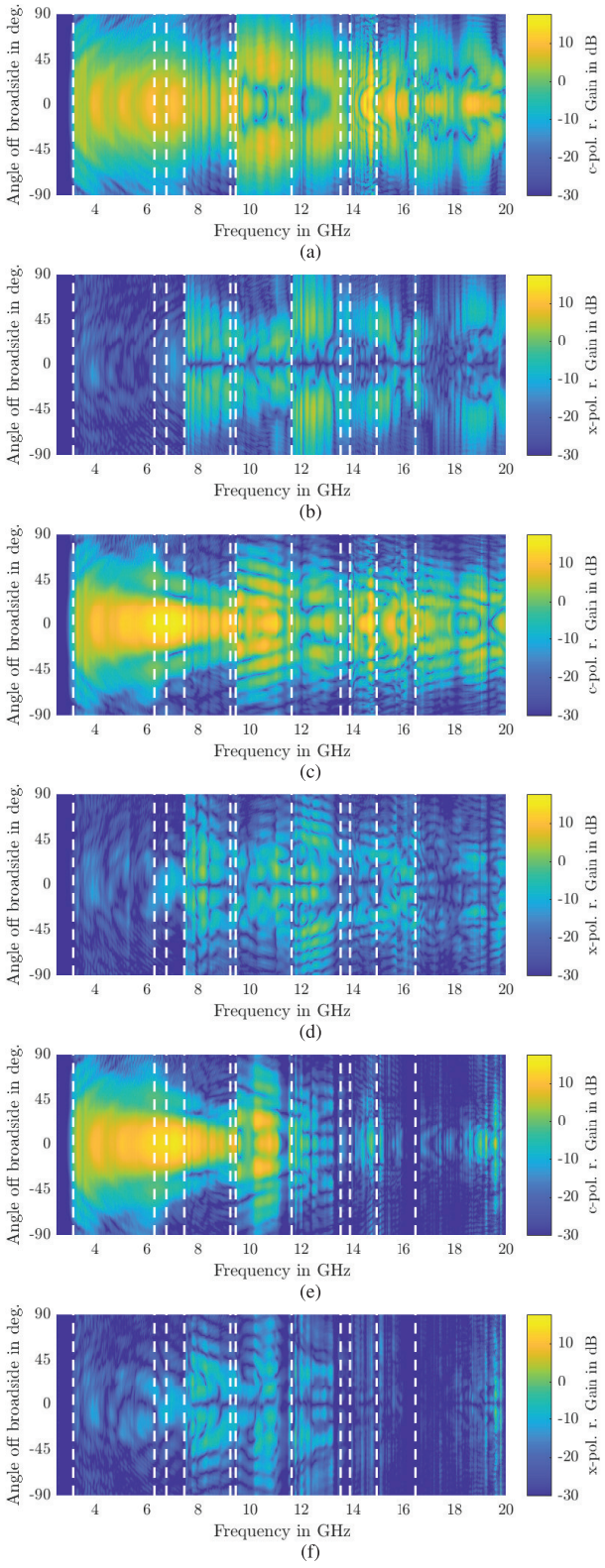

Fig. 11. H-plane co- (a), (c), and (e), and cross-polarized (b), (d), and (f), realized gain measurements as a function of frequency and angle of broadside for (a) and (b) standalone RWG, (c) and (d) solid dielectric rod and (e) and (f) woodpile dielectric rod antenna with the cut-off frequencies of individual higher order modes in the waveguide plotted in dashed white lines.

in the measurements. The coaxial transition primarily supports the fundamental TE_{10} mode, which explains the high

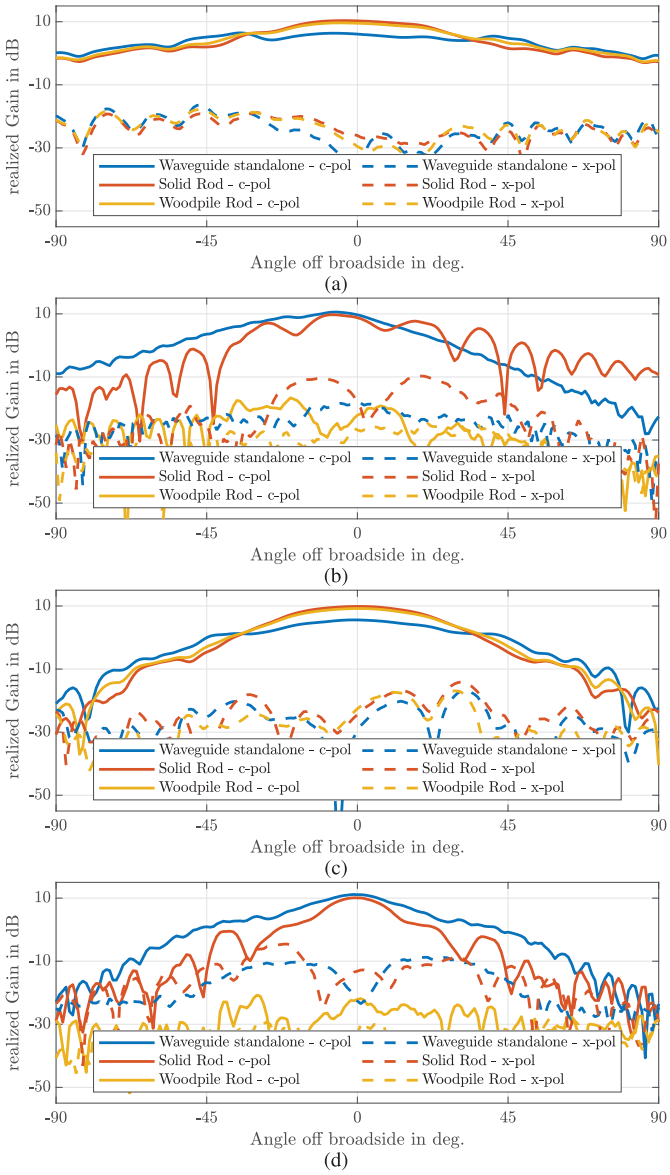

Fig. 12. Comparison of measured co-(solid lines) and cross-polarized (dashed lines) realized gain values in the E- (a) and (b) and H-plane (c) and (d) for the standalone RWG (blue), solid dielectric rod (red) and woodpile dielectric rod (yellow) antenna as a function of angle off broadside for (a) and (c) 5 GHz and (b) and (d) 15 GHz.

reflections for frequencies above 7 GHz compared to the simulation result presented in Fig. 6(a), as the simulation only considers the fundamental mode. Furthermore, compared to simulations, we do not measure the almost 0 dB reflection coefficient for the woodpile dielectric rod at the third harmonic as predicted by simulations. This can, again, be attributed to the feed primarily supporting the fundamental mode, as scattering from the woodpile excites a plethora of higher order modes as demonstrated with the multimode simulations in the previous section. This leads to a "ping-pong" of the energy contained in the higher order modes between the waveguide feed and the woodpile rod and a subsequent dissipation due to the conductive and dielectric losses. Due to the limitations of the waveguide feed, the effect of the solid dielectric rod compared to the woodpile rod can be best observed considering the realized gain measurements in the E- and H-plane

as a function of frequency and the angle off broadside for all three antenna configurations presented in Figs. 10– 12. As expected at the design frequency 5 GHz, the solid rod and woodpile rod behave almost identically and increase the gain compared to the standalone RWG. At the third harmonic frequency, the comparison between the solid and woodpile rod presents a drastic reduction in the realized gain of up to 35 dB corresponding again well to the expected results from the simulations. Although the presented experimental results confirm the antenna's operational principle, one can observe oscillations in the input reflection coefficient and realized gain values as a function of frequency. This phenomenon is present even in the standalone waveguide measurement. We attribute this effect to an issue with coaxial waveguide transition, which results in poor matching. An alternative explanation could be an interaction of the antenna under test with the mounting equipment in the anechoic chamber.

VII. Conclusion

This work introduces a novel concept to mitigate the unintended transmission and reception of signals at the third harmonic of dielectric rod antennas without requiring additional components or complex feed networks. The presented antenna exploits the concept of a bandgap dielectric crystal with a woodpile unit cell that behaves like an effective material at the design frequency but exhibits a complete 3-D bandgap at the third harmonic. Numerical simulations confirm the operational principle of the antenna and show a significant drop in the realized gain and overall radiated power at the third harmonic. Unexpected behavior of the bandgap rod antenna at intermediate frequencies between the fundamental and third harmonic are investigated and linked to the excitation of higher order modes in the waveguide due to scattering off the periodic structure. The operational principle of the antenna is confirmed in experiments via the characterization of the input reflection coefficients and far-field radiation patterns of a traditional rod antenna and its bandgap counterpart.

Reference

[1] S. Keyrouz and D. Caratelli, "Dielectric resonator antennas: Basic concepts, design guidelines, and recent developments at millimeter-wave frequencies," *Int. J. Antennas Propag.*, vol. 2016, pp. 1–20, Jan. 2016, doi: 10.1155/2016/6075680.

[2] S. P. Hehenberger, S. Caizzone, and A. G. Yarovoy, "Additive manufacturing of linear continuous permittivity profiles and their application to cylindrical dielectric resonator antennas," *IEEE Open J. Antennas Propag.*, vol. 4, pp. 373–382, 2023, doi: 10.1109/OJAP.2023.3258147.

[3] G. Saffold, "Theory and application of dielectric rod antennas and arrays," Ph.D. dissertation, Dept. Elect. Eng., USF Tampa Graduate, Tampa, FL, USA, 2021. [Online]. Available: https://digitalcommons.usf.edu/etd/8857/

[4] S. Kwon, B. M. Lee, Y. J. Yoon, W. Y. Song, and J.-G. Yook, "A harmonic suppression antenna for an active integrated antenna," *IEEE Microw. Wireless Compon. Lett.*, vol. 13, no. 2, pp. 54–56, Feb. 2003, doi: 10.1109/lmwc.2003.808716.

[5] S. Kwon, H. K. Yoon, and Y. J. Yoon, "Harmonic tuning antennas using slots and short-pins," in *IEEE Antennas Propag. Soc. Int. Symp. Dig.*, vol. 1, Jul. 2001, pp. 118–121, doi: 10.1109/APS.2001.958807.

[6] Y. Horii and M. Tsutsumi, "Harmonic control by photonic bandgap on microstrip patch antenna," *IEEE Microw. Guided Wave Lett.*, vol. 9, no. 1, pp. 13–15, Jan. 1999, doi: 10.1109/75.752109.

[7] E. Yablonovitch, "Inhibited spontaneous emission in solid-state physics and electronics," *Phys. Rev. Lett.*, vol. 58, no. 20, pp. 2059–2062, May 1987, doi: 10.1103/physrevlett.58.2059.

[8] I. Ederra et al., "Electromagnetic-bandgap waveguide for the millimeter range," *IEEE Trans. Microw. Theory Techn.*, vol. 58, no. 7, pp. 1734–1741, Jul. 2010, doi: 10.1109/TMTT.2010.2050098.

[9] J. D. Joannopoulos, S. G. Johnson, J. N. Winn, and R. D. Meade, *Photonic Crystals*. Princeton, NJ, USA: Princeton Univ. Press, 2011, doi: 10.2307/j.ctvcm4gz9.

[10] Y. T. Lo and S. W. Lee, *Antenna Handbook*. Cham, Switzerland: Springer, doi: 10.1007/978-1-4615-2638-4.

[11] F. Yang and Y. Rahmat-Samii, "Surface wave antennas," in *Electromagnetic Band Gap Structures in Antenna Engineering*. Cambridge, U.K.: Cambridge Univ. Press, 2008, pp. 203–237, doi: 10.1017/cbo9780511754531.008.

[12] Y. Wu, D. Isakov, and P. Grant, "Fabrication of composite filaments with high dielectric permittivity for fused deposition 3D printing," *Materials*, vol. 10, no. 10, p. 1218, Oct. 2017, doi: 10.3390/ma10101218.

[13] S. P. Hehenberger, S. Caizzone, S. Thurner, and A. G. Yarovoy, "Broadband effective permittivity simulation and measurement techniques for 3-D-printed dielectric crystals," *IEEE Trans. Microw. Theory Techn.*, vol. 71, no. 10, pp. 4161–4172, Oct. 2023, doi: 10.1109/TMTT.2023.3259479.

Simon P. Hehenberger (Graduate Student Member, IEEE) received the B.Sc. and M.Sc. degrees in electronics and information technology from Johannes Kepler University, Linz, Austria, in 2017 and 2020, respectively. In 2021, he became an external Ph.D. Student with the Microwave Sensing, Signals, and Systems Group, TU Delft, Delft, The Netherlands.

During his studies, he focused on high-frequency systems and radar while completing his master's thesis about the design, simulation, and test of a fully functional FMCW–MIMO radar system with nonuniform arrays and substrate integrated waveguides. In 2020, he joined the Institute for Communication and Navigation, German Aerospace Center, Wessling, Germany, where he works on miniaturized dielectric resonator antennas, arrays, and methods for array decoupling with a focus on satellite navigation applications. In his Ph.D. project, he explores the potential of additive manufacturing with respect to high-frequency components and antenna systems.

Stefano Caizzone (Member, IEEE) received the M.Sc. degree in telecommunications engineering and the Ph.D. degree in geoinformation from the University of Rome Tor Vergata, Rome, Italy, in 2009 and 2015, respectively.

Since 2010, he has been with the Antenna Group, German Aerospace Center (DLR), Wessling, Germany, where he has been responsible for the development of innovative miniaturized antennas. Since July 2020, he leads the Antenna Systems Group. His main research interests concern small antennas for satellite navigation, controlled radiation pattern antennas for robust satellite navigation and high-performance antenna design for precise satellite navigation, antenna arrays for satellite communication, and installed performance analysis.

Alexander Yarovoy (Fellow, IEEE) received the diploma degree (Hons.) in radiophysics and electronics. He is a candidate of Physics and Mathematical Sciences and Doctor of Physics and Mathematical Sciences degrees in radiophysics from Kharkov State University, Kharkiv, Ukraine, in 1984, 1987, and 1994, respectively.

In 1987, he joined the Department of Radiophysics, Kharkov State University, as a Researcher and became a Full Professor in 1997. From September 1994 to 1996, he was with the Technical University of Ilmenau, Ilmenau, Germany, as a Visiting Researcher. Since 1999, he has been with Delft University of Technology, Delft, The Netherlands. Since 2009, he leads there a Chair of Microwave Sensing, Systems and Signals. His main research interests are in high-resolution radar, microwave imaging, and applied EMs (in particular, UWB antennas). He has authored and coauthored more than 500 scientific or technical articles, seven patents, and 14 book chapters.

Prof. Yarovoy was a recipient of the European Microwave Week Radar Award for the paper that best advances the state-of-the-art in radar technology in 2001 (together with L.P. Ligthart and P. van Genderen) and in 2012 (together with T. Savelyev). In 2010 together with D. Caratelli, he got the best paper award of the Applied Computational Electromagnetic Society (ACES). He served as a General TPC Chair for the 2020 European Microwave Week (EuMW'20), as the Chair and the TPC Chair for the 5th European Radar Conference (EuRAD'08), and the Secretary for the 1st European Radar Conference (EuRAD'04). He served also as the Co-Chair and TPC Chair for the Xth International Conference on GPR (GPR2004). He serves as an Associate editor for the IEEE Transaction on Radar Systems. From 2011 to 2018, he served as an Associate Editor for the *International Journal of Microwave and Wireless Technologies*. From 2008 to 2017, he served as the Director for the European Microwave Association (EuMA).